Cell

Coordination of Kinase and Phosphatase Activities by Lem4 Enables Nuclear Envelope Reassembly during Mitosis

Claudio Asencio,[1,3,4] Iain F. Davidson,[1,3] Rachel Santarella-Mellwig,[1] Thi Bach Nga Ly-Hartig,[1] Moritz Mall,[1] Matthew R. Wallenfang,[2] Iain W. Mattaj,[1,*] and Mátyás Gorjánácz[1]
[1]European Molecular Biology Laboratory, Meyerhofstrasse 1, 69117 Heidelberg, Germany
[2]The Johns Hopkins University School of Medicine, 725 North Wolfe Street, Baltimore, MD 21205, USA
[3]These authors contributed equally to this work
[4]Present address: Centro Andaluz de Biología del Desarrollo and Centro de Investigación Biomédica en Red: Enfermedades Raras, Instituto de Salud Carlos III, Universidad Pablo de Olavide-Consejo Superior de Investigaciones Científicas, Ctra. de Utrera Km 1, 41013 Sevilla, Spain
*Correspondence: mattaj@embl.org
http://dx.doi.org/10.1016/j.cell.2012.04.043

SUMMARY

Mitosis in metazoa requires nuclear envelope (NE) disassembly and reassembly. NE disassembly is driven by multiple phosphorylation events. Mitotic phosphorylation of the protein BAF reduces its affinity for chromatin and the LEM family of inner nuclear membrane proteins; loss of this BAF-mediated chromatin-NE link contributes to NE disassembly. BAF must reassociate with chromatin and LEM proteins at mitotic exit to reform the NE; however, how its dephosphorylation is regulated is unknown. Here, we show that the *C. elegans* protein LEM-4L and its human ortholog Lem4 (also called ANKLE2) are both required for BAF dephosphorylation. They act in part by inhibiting BAF's mitotic kinase, VRK-1, in vivo and in vitro. In addition, Lem4/LEM-4L interacts with PP2A and is required for it to dephosphorylate BAF during mitotic exit. By coordinating VRK-1- and PP2A-mediated signaling on BAF, Lem4/LEM-4L controls postmitotic NE formation in a function conserved from worms to humans.

INTRODUCTION

The nuclear envelope (NE) comprises inner and outer nuclear membranes (INM and ONM) that fuse at nuclear pore complexes (NPCs), large multiprotein complexes through which all nucleocytoplasmic transport occurs (Hetzer et al., 2005). The ONM is continuous with the endoplasmic reticulum (ER), whereas the INM harbors a discrete set of transmembrane proteins; in metazoa, many of these contact the nuclear lamina, an intermediate filament meshwork that underlies the NE (Burke and Ellenberg, 2002). In metazoa, the NE is broken down upon entry into mitosis and is reformed upon mitotic exit; how this happens is not fully understood (Güttinger et al., 2009).

The LEM domain protein family shares an ~40 amino acid domain first identified in the proteins *L*ap2, *E*merin, and *M*an1 (Lin et al., 2000). Most LEM proteins contain transmembrane domains, reside in the INM, and interact with the nuclear lamina (Wagner and Krohne, 2007). One described function of the LEM domain is to interact with the highly conserved chromatin-binding protein barrier-to-autointegration factor (BAF) (Wagner and Krohne, 2007). During interphase, the localization of LEM proteins Lamin A and BAF is mutually dependent; depletion of BAF or overexpression of a BAF mutant deficient in DNA binding results in the mislocalization of LEM proteins and Lamin A, whereas depletion of Lamin A leads to mislocalization of BAF and LEM proteins, and depletion of LEM proteins causes mislocalization of BAF (Ulbert et al., 2006; Margalit et al., 2007; Haraguchi et al., 2008). BAF functions in the regulation of chromatin structure and chromosome segregation (Margalit et al., 2007) and also in gene expression and development (Wagner and Krohne, 2007), and it is essential for postmitotic NE reformation in *C. elegans* (Gorjánácz et al., 2007) and during *Drosophila* meiosis (Lancaster et al., 2007). BAF-LEM interactions are thus an important link between chromatin and the NE, both through the maintaining nuclear organization and during postmitotic NE reassembly.

The localization of BAF changes during the cell cycle. In interphase, BAF is concentrated at the nuclear periphery and interacts with LEM proteins (Haraguchi et al., 2001; Shimi et al., 2004; Margalit et al., 2005). During early mitosis, BAF is distributed uniformly throughout the cell. After the metaphase-anaphase transition, BAF associates with chromatin and becomes concentrated at the "core" region of chromosomes surrounding the centromeres where its mobility, and the mobility of LEM proteins, significantly decreases (Haraguchi et al., 2008).

NE breakdown (NEBD) and reformation are controlled by protein phosphorylation. Members of the vaccinia-related kinase (VRK) family of mitotic kinases phosphorylate BAF in mitosis and meiosis; this modification strongly reduces the affinity of BAF for chromatin and slightly weakens its affinity for LEM proteins (Margalit et al., 2007). Overexpression of VRK-1 releases BAF from chromatin in human cells (Nichols et al., 2006), whereas depletion of VRK-1 in *C. elegans* prevents the release of BAF

from chromatin upon mitotic entry and leads to defects in chromosome segregation (Gorjánácz et al., 2007). Phosphorylation of BAF by VRK-1 upon entry into mitosis is therefore proposed to break the link between chromatin, BAF, and LEM proteins. The mechanism that permits BAF to reassociate with chromatin at mitotic exit is unclear.

Protein phosphatases regulate numerous processes during mitotic progression, but their roles in mitotic exit are mostly uncharacterized (Bollen et al., 2009; Wurzenberger and Gerlich, 2011). A PP1/Repo-Man complex dephosphorylates histone H3 and potentially other substrates and, by a mechanism that is not yet completely understood, influences mitotic exit (Vagnarelli et al., 2011). Also, a protein phosphatase 2A (PP2A) complex comprising PP2A-CA, PP2A-R1A, and PP2A-B55α regulates mitotic exit in human cells, although the target or targets of this complex are unknown (Schmitz et al., 2010).

Here, we show that PP2A regulates BAF chromatin recruitment during mitotic exit and is required to enable BAF's essential function in NE assembly. In addition, we show that Lem4 is essential for BAF recruitment to chromatin upon mitotic exit in *C. elegans* and human cells. Lem4 depletion or mutation causes NE morphology defects and BAF hyperphosphorylation. In vivo and in vitro data show that BAF phosphorylation is dependent on VRK-1 and is counteracted by PP2A. We propose an evolutionarily conserved model whereby Lem4 coordinates the control of BAF dephosphorylation by interacting with and inhibiting VRK-1 and by supporting PP2A action on BAF. This results in BAF dephosphorylation and chromatin recruitment, thereby facilitating NE assembly. Such coordination may be more generally employed during mitotic exit because a recent kinome analysis revealed that many kinases and phosphatases reside in cocomplexes (Breitkreutz et al., 2010).

RESULTS

Identification of the *C. elegans lem-4L* Gene

To study postmitotic NE formation, we screened *C. elegans* strains harboring temperature-sensitive maternal effect embryonic lethal mutations (Golden et al., 2000) and identified four mutations causing nuclear appearance defects (Figures S1A–S1E available online). SNP mapping and sequencing revealed that three lines, *ax146*, *ax545*, and *ax640*, were mutated in three genes previously implicated in nuclear assembly, *npp-8*, *ima-2*, and *mel-28*, respectively (Galy et al., 2003; Franz et al., 2005; Askjaer et al., 2002; Galy et al., 2006; Fernandez and Piano, 2006). In the *ax475* line, a point mutation was mapped to the uncharacterized Y55F3BR.8 gene. Bidirectional BLAST-P analysis revealed Lem4 (also known as ANKLE2) as the closest human gene, with 33% sequence identity and 49% sequence similarity over a 364 amino acid region (Figure S1F). The Lem4 protein has a predicted transmembrane region at its N terminus, followed by an LEM domain and ankyrin repeats. Y55F3BR.8 is similar in organization and predicted secondary structure, but we were unable to identify a LEM domain in the *C. elegans* protein. We therefore refer to Y55F3BR.8 as LEM-4Like (LEM-4L) and to the homozygous mutant *ax475* embryos as *lem-4L(ax475)*. The *lem-4L(ax475)* mutant carries an Ala to Val missense mutation at the conserved position 229 (Figure S1F).

Both LEM-4L and Lem4 Are Required for NE Formation

Homozygous mutant *lem-4L(ax475)* worms were 93% ± 4% (n = 407) viable at 16°C and had normal nuclei (Figures S1A and S1C). At 25°C, *lem-4L(ax475)* embryos (n = 454) died early during development and displayed severe nuclear appearance defects (Figure S1C, arrows). In *lem-4L(ax475)* embryos at 16°C, Lamin (LMN-1) and nucleoporins (mAb414, NUP96, and NUP107) formed a sharp NE rim, like wild-type (Figures 1A, S2A, and S2B). At 25°C, the NE proteins were abnormally distributed (Figures 1A, S2A, and S2B, third columns). LEM-4L protein levels in *lem-4L(ax475)* embryos at 16°C and 25°C were 26.8% ± 8.4% and 5.2% ± 3.9% (n = 3) of wild-type (Figure 1B). To confirm that the defects were due to *lem-4L* mutation, *lem-4L(ax475)* worms were transformed with the wild-type *lem-4L* gene. The transformed embryos were viable at restrictive temperature with wild-type nuclei (Figure 1A, fourth column).

Depletion of *lem-4L* from embryos by RNA interference (RNAi) resulted in less severe NE defects than those observed in the *lem-4L(ax475)* mutant at 25°C (Figures 1C and S1G). Western blotting showed that the LEM-4L protein level in *lem-4L(RNAi)* embryos was 20.2% ± 4.2% (n = 3) of wild-type (Figure 1B).

Immunostaining of control embryos with anti-LEM-4L antibodies and expression of a LEM-4L-GFP fusion construct revealed that the protein is enriched at the NE (Figures 1C and S2C); reduction of the anti-LEM-4L signal in *lem-4L(RNAi)* or *lem-4L(ax475)* embryos (Figure 1C) confirmed the specificity of the antibodies.

We next characterized human Lem4. Anti-Lem4 antibodies recognized a protein of ~100 kDa (Figure S2D). Endogenous Lem4 and overexpressed GFP-tagged Lem4 (Figures S2E and S2F) localized to the ER in HeLa cells fixed by several methods, which is a surprising finding given that all previously characterized transmembrane LEM domain proteins localize to the INM (Wagner and Krohne, 2007). Differential permeabilization followed by immunostaining revealed that the C terminus of Lem4 is cytoplasmic (Figure S2E).

Lem4 protein levels in human cells were efficiently reduced by using two small interfering RNA (siRNA) oligos (Figure S2G). Cells depleted of Lem4 showed normal recruitment of NPCs and NE proteins, but 20%–30% showed nuclear shape defects (Figure 1D; data not shown) similar to those observed upon Lem2 depletion (Ulbert et al., 2006). To determine the specificity of the depletion phenotype, we generated a HeLa H2B-mCherry cell line that stably expressed an myc-tagged RNAi-insensitive version of Lem4 (H2B-mCherry/Lem4-myc). H2B-mCherry cells depleted of Lem4 displayed abnormal nuclear shape (Figure 1E, top), whereas H2B-mCherry/Lem4-myc expressing cells did not (Figure 1E, bottom; quantification Figure 1F). Lem4-myc expression was confirmed by using Lem4 and myc antibodies (Figures 1E and 1G; data not shown). Western blotting confirmed that endogenous Lem4 was depleted from both cell lines and that exogenous Lem4-myc is resistant to RNAi treatment (Figure 1G).

Interestingly, Lem4-myc migrated faster than endogenous Lem4 upon SDS-PAGE (Figure 1G). Lem4-myc complementary DNA (cDNA) was cloned and sequenced; Lem4-myc was found to lack aa 256–646, a deletion that might be due to alternative splicing or rearrangement of the transfected DNA (Figure S2H). We were unable to isolate stable cell lines that efficiently and

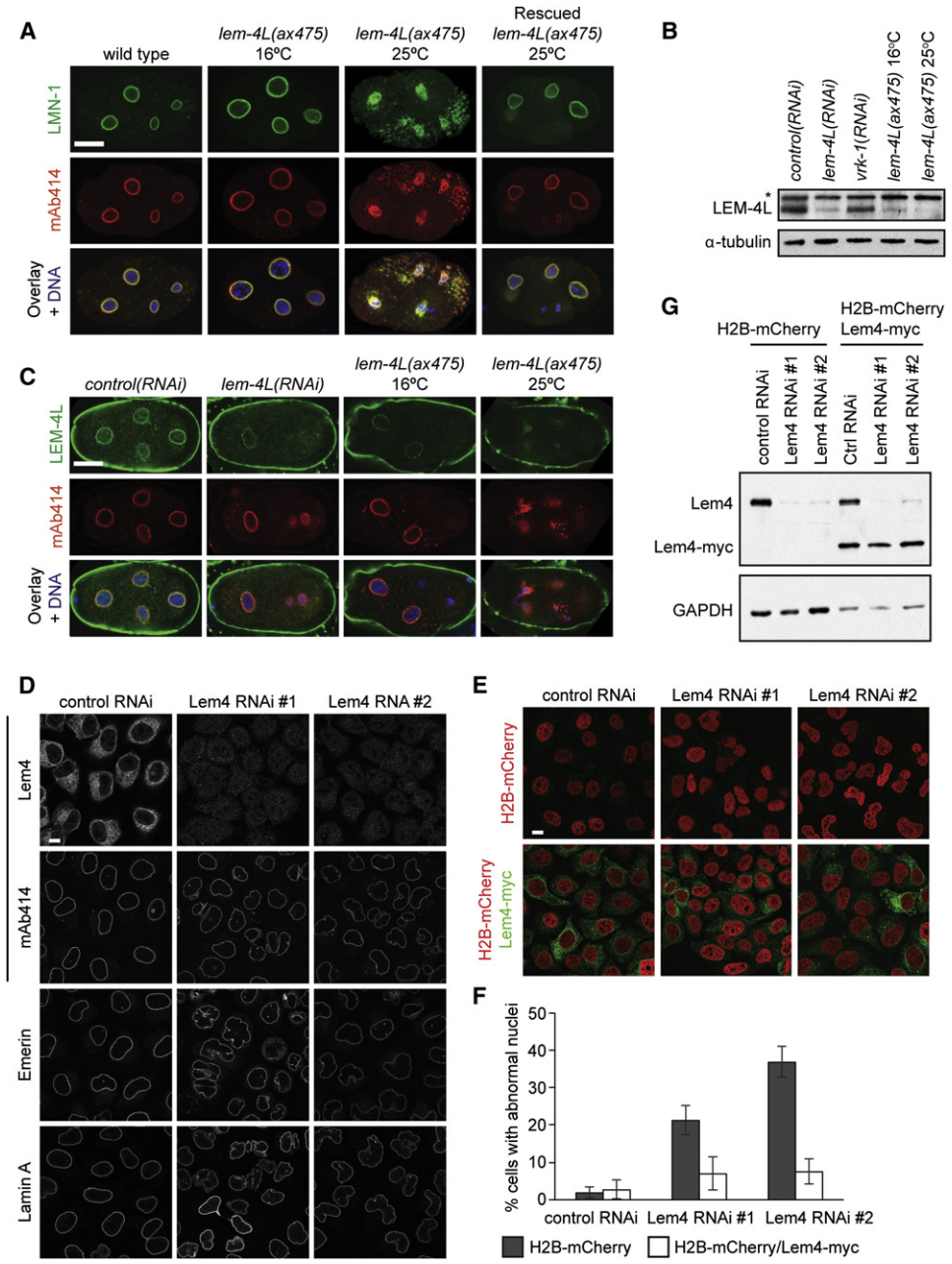

Figure 1. Depletion of Worm LEM-4L or Human Lem4 Results in Abnormal Nuclear Morphology

(A) Wild-type, *lem-4L(ax475)*, and rescued *lem-4L(ax475)* embryos were grown at 16 or 25°C and stained with anti-LMN-1 (green), mAb414 (red), or Hoechst DNA stain (blue). Scale bar, 10 μm.

(B) *control(RNAi)*, *lem-4L(RNAi)*, *vrk-1(RNAi)*, and *lem-4L(ax475)* embryos were grown at 16 or 25°C and processed for western blotting with anti-LEM-4L or anti-α–tubulin. Asterisk, cross-reacting band.

(C) *control(RNAi)*, *lem-4L(RNAi)*, and *lem-4L(ax475)* embryos grown at 16 or 25°C were stained with anti-LEM-4L (green) and mAb414 (red). Scale bar, 10 μm.

(D) HeLa cells were transfected with control siRNA or with either Lem4 oligo 1 or Lem4 oligo 2 siRNA. After 48 hr, cells were costained (Lem4, mAb414) or stained with the indicated antibodies.

(E) HeLa cells stably expressing H2B-mCherry (top row) or H2B-mCherry and Lem4-myc (bottom row) were transfected with control, Lem4 oligo 1, or 2 siRNAs. After 48 hr, both cell lines were stained with anti-myc (green). H2B-mCherry was used to visualize DNA (red).

(F) The percentage of cells (average of four independent experiments, $n \geq 100$ cells per experiment) displaying abnormal nuclear shape after RNAi treatment was determined visually. Error bars represent SD.

(G) In parallel, cells were resuspended in SDS-PAGE sample buffer and western blotted by using affinity-purified Lem4 antibody. Lower band, truncated Lem4-myc. GAPDH, loading control.

See also Figures S1 and S2 and Tables S1, S2, and S3.

homogenously express full-length Lem4, suggesting that its overexpression is deleterious. However, the truncated form of Lem4 rescued the NE shape defects. This deletion removes the bulk of the amino acid sequence most highly conserved between Lem4 and LEM-4L, raising the possibility that Lem4 and LEM-4L may affect nuclear shape through regions dissimilar in amino acid sequence. Thus, efficient reduction or loss of human Lem4 or *C. elegans* LEM-4L results in defects in the NE.

LEM-4L and Lem4 Regulate BAF during Mitosis

A function of the LEM domain is to interact with BAF. To investigate a potential link between LEM-4L and BAF-1, we compared nuclei in *lem-4L(ax475)* and *baf-1(t1639)* (Gorjánácz et al., 2007) mutant embryos by transmission electron microscopy (TEM). Wild-type and *lem-4L(ax475)* mutant nuclei at 16°C were enclosed by a continuous NE membrane (Figures 2A and 2B). At 16°C, *lem-4L(ax475)* mutant embryos displayed minor defects in INM-ONM spacing, whereas at 25°C, the NE of both *lem-4L(ax475)* and *baf-1(t1639)* mutant embryos was similarly disorganized (Figures 2C–2E; Gorjánácz et al., 2007). Their nuclei were multilobed, and, although the NE membranes were adjacent to the chromatin, they were not organized into a closed NE.

BAF-1 is required during anaphase to organize membranes into a closed NE (Gorjánácz et al., 2007). We therefore analyzed the localization of GFP-BAF-1 during the cell cycle in the absence of LEM-4L (Figures 2G, S3A, and S3B). In control embryos (n = 18), GFP-BAF-1 left chromatin during mitosis and was recruited back 60 s after anaphase onset. GFP-BAF-1 recruitment at the nuclear periphery peaked 80–100 s after anaphase onset (Figures 2G and S3A). On completion of NE assembly, 140 s after anaphase onset, GFP-BAF-1 intensity dropped to a level that was constant during interphase. The early strong recruitment of GFP-BAF-1 did not occur after LEM-4L RNAi (n = 16); instead, BAF-1 was recruited gradually for 120–140 s after anaphase onset (Figures 2G and S3B). The interphase NE level of GFP-BAF-1 was unaffected. Downregulation of LEM-3 (n = 8), LEM-2 (n = 8), and EMR-1 (n = 10) LEM proteins (Figures S3C–S3E) did not decrease anaphase recruitment of BAF-1, although LEM-2 and EMR-1 downregulation decreased interphase NE levels of BAF-1 (Figures 2H–2J and S3C–S3E). Thus, LEM proteins are differentially required to regulate BAF-1 localization during the cell cycle.

To examine human cells, we generated a cell line that stably expressed GFP-BAF and H2B-mCherry, depleted Lem4 by RNAi, and followed GFP-BAF chromatin recruitment in anaphase by time-lapse microscopy. Control depletions allowed typical BAF recruitment (Haraguchi et al., 2001, 2008; Shimi et al., 2004;), with strong recruitment of BAF to chromatin ~6 min after anaphase onset, gradual NE relocalization during telophase, and maintenance of nuclear and cytoplasmic pools (Figures 2K and S3F). Lem4-depleted cells, but not Lem2- or Emerin-depleted cells, showed decreased and delayed GFP-BAF recruitment during mitotic exit (Figures 2K, 2L, S3G, and S3H). Thus, both Lem4 and LEM4-L, but not other Lem proteins, are required for BAF recruitment to chromatin during mitotic exit.

vrk-1 Mutation Suppresses *lem-4L(ax475)*

To further study *lem-4L* function during NE assembly, we performed a suppressor screen. We mutagenized *lem-4L(ax475)* worms and identified a *lem-4L(ax475)* mutant line that grew and reproduced at 25°C (72.5% ± 9.5% fertile [n = 40]). Wild-type, *lem-4L(ax475)*, and suppressor embryos were grown at 25°C and EMR-1 and nucleoporins were immunostained. Nuclei in the suppressor strain were indistinguishable from wild-type (Figure 3A, third column; data not shown). In addition, TEM of the suppressed *lem-4L(ax475)* embryos confirmed that NE structure was wild-type (Figure 2F).

The suppressor mutation caused a C to T transition in nucleotide 206 of the *vrk-1* gene, changing amino acid 69 in the kinase domain of VRK-1 from Pro to Leu. The allele is named *vrk-1(x1)*. To confirm that *vrk-1(x1)* is responsible for *lem-4L(ax475)* suppression, we downregulated VRK-1 by RNAi in wild-type and *lem-4L(ax475)* mutants grown at 16°C and 25°C and monitored embryonic lethality. *vrk-1* RNAi resulted in almost complete embryonic lethality in wild-type worms but in suppression of lethality in *lem-4L(ax475)* mutants at 25°C (Figure 3B, middle). Silencing of *vrk-1* in *lem-4L(ax475)* worms at 16°C resulted in intermediate lethality (Figure 3B, right). This confirms that *vrk-1(x1)* suppresses *lem-4L(ax475)*.

To analyze the effect of *vrk-1(x1)*, we immunostained VRK-1 and nucleoporins in wild-type, *lem-4L(ax475)*, and suppressor embryos. The *vrk-1* mutation did not affect either VRK-1 expression or localization to the NE during prophase (Figures 3C and 3D). These results, together with the observed reduced embryonic lethality (87.5% ± 5.7%; n = 442) compared to *vrk-1(RNAi)*, suggest that *vrk-1(x1)* is not null.

VRK-1 and LEM-4L Divergently Regulate BAF-1 Phosphorylation

Phosphorylation of BAF-1 by VRK-1 is necessary for its removal from chromatin during mitosis. BAF-1 dephosphorylation might therefore be required for chromatin rebinding during mitotic exit. To determine whether LEM-4L might affect BAF-1 phosphorylation, we performed 2D western blots. In *control* embryonic extracts, four spots were recognized by BAF-1 antibodies (Gorjánácz et al., 2007). Two are known phosphoisoforms (Figure 4A, spots 2 and 3), and spot 4 is likely a BAF-1 dimer. In *lem-4L(RNAi)* embryonic extract, the altered balance between the unphosphorylated (spot 1) and phosphorylated forms indicated that BAF-1 was more phosphorylated (Figures 4A and 4B). In contrast, downregulation of *lem-3*, *lem-2*, or *emr-1* had no effect on BAF-1 phosphorylation (Figures 4A and 4B; data not shown).

To confirm the opposing functions of LEM-4L and VRK-1 on BAF-1 phosphorylation, we analyzed the phosphorylation state of BAF-1 in wild-type, *lem-4L(ax475)*, and *vrk-1(x1)* single mutants and in a *lem-4L(ax475); vrk-1(x1)* double mutant with and without *lem-4L* and *vrk-1* RNAi (Figures 4C and 4D). A reduction in LEM-4L resulted in hyperphosphorylation of BAF-1. The increase in BAF-1 phosphorylation levels ranged from 2-fold (Figure 4D; *lem-4L(RNAi)*) to 28-fold [Figure 4D; *lem-4L(ax475)* and *lem-4L(ax475); lem-4(RNAi)*] of wild-type. *lem-4L* RNAi did not increase BAF-1 phosphorylation levels in *lem-4L(ax475)* mutant worms, suggesting that the *lem-4(ax475)* mutation inactivates LEM4-L at 25°C. In contrast, reduction of VRK-1 resulted in the hypophosphorylation of BAF-1. Combinatorial reduction of both VRK-1 and LEM-4L resulted in a balance among BAF-1

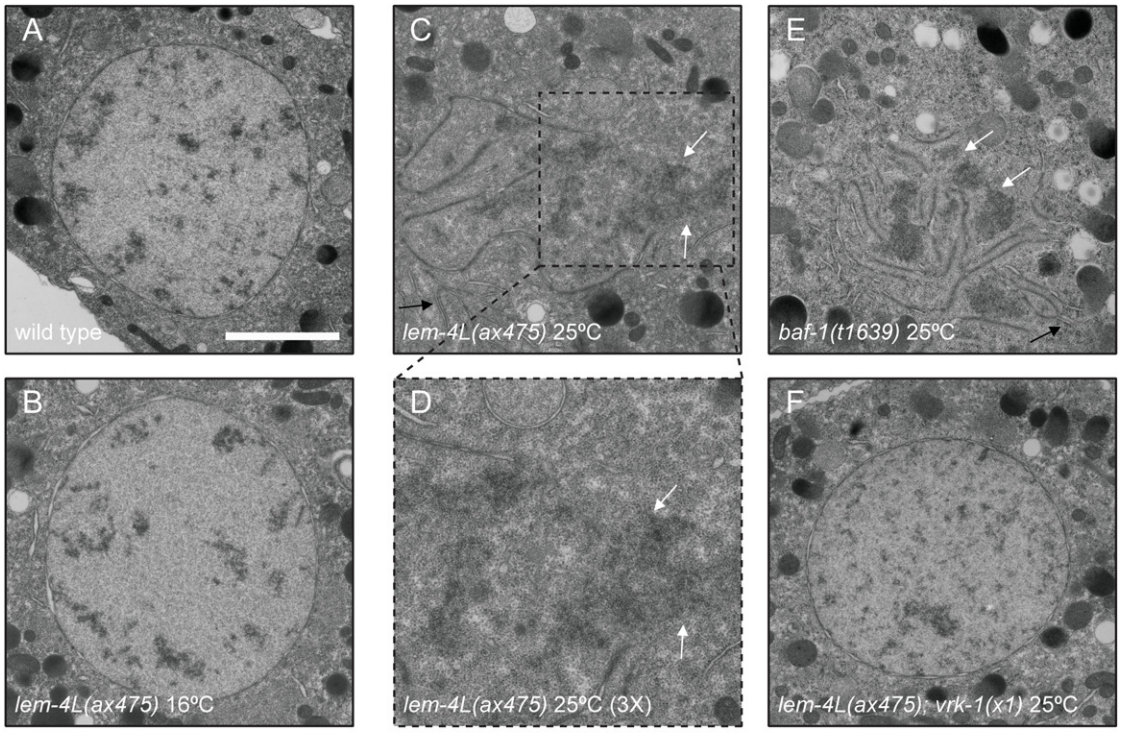
A
wild type
C
lem-4L(ax475) 25ºC
E
baf-1(t1639) 25ºC
B
lem-4L(ax475) 16ºC
D
lem-4L(ax475) 25ºC (3X)
F
lem-4L(ax475); vrk-1(x1) 25ºC

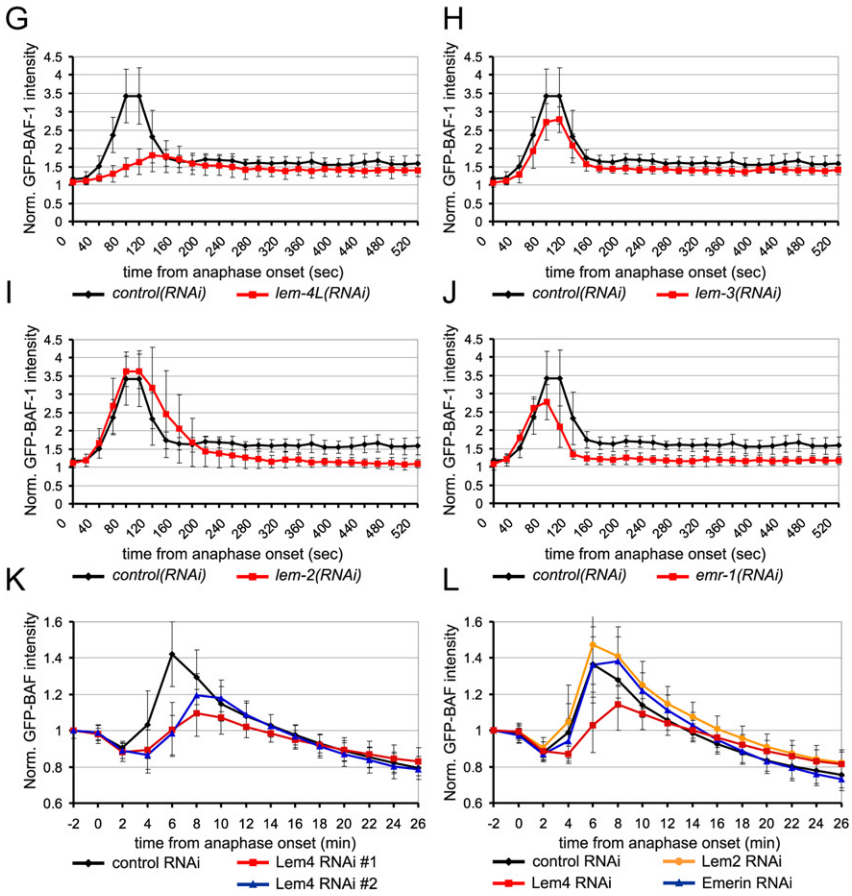
G
H
Norm. GFP-BAF-1 intensity
time from anaphase onset (sec)
I
control(RNAi)
lem-4L(RNAi)
J
lem-3(RNAi)
K
lem-2(RNAi)
L
emr-1(RNAi)
Norm. GFP-BAF intensity
time from anaphase onset (min)
control RNAi
Lem4 RNAi #1
Lem4 RNAi #2
Lem2 RNAi
Lem4 RNAi
Emerin RNAi

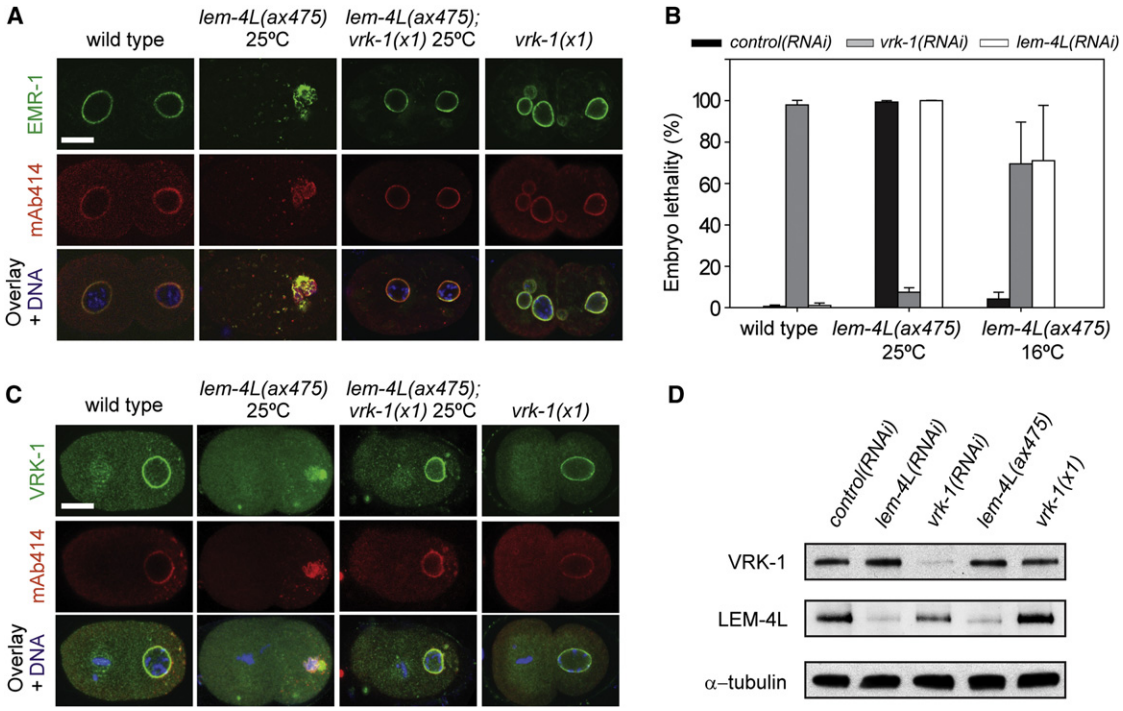

Figure 3. A *vrk-1* Mutation Suppresses *lem-4L(ax475)*

(A and C) Wild-type, *lem-4L(ax475)*, *lem-4L(ax475); vrk-1(x1)* double mutant and *vrk-1(x1)* embryos were stained with mAb414 (red) and EMR-1 (green) (A) or VRK-1 (green) (C) antibodies. Scale bars, 10 μm.

(B) Wild-type and *lem-4L(ax475)* worms were grown at 16 or 25°C and subjected to control, *vrk-1*, or *lem-4L* RNAi. Embryonic lethality was determined in 10 worms per condition in three independent experiments. Error bars represent SD.

(D) Anti-LEM-4L and anti-VRK-1 antibodies were used to determine LEM-4L and VRK-1 protein levels in *control(RNAi)*, *lem-4L(RNAi)*, *vrk-1(RNAi)*, *lem-4L(ax475)*, and *vrk-1(x1)* embryos. Anti-α-tubulin was a control.

See also Table S2.

isoforms that also allowed survival and explained the suppression of *lem-4L(ax475)* by *vrk1(x1)*.

LEM-4L and Lem4 Inhibit VRK-1 Phosphorylation of BAF-1

The divergent effects of LEM4-L and VRK-1 on BAF-1 phosphorylation in vivo suggested that Lem4 might reverse BAF-1 phosphorylation by VRK-1. To test for Lem4-VRK-1 physical interaction, we performed GST pull-down experiments using purified proteins. Human Lem4 aa 59–938 and *C. elegans* LEM-4L aa 257–600 bound VRK-1-GST, but not GST alone (Figure 5A).

We then performed in vitro kinase assays to monitor the effect of Lem4 on BAF-1 phosphorylation by VRK-1. Whereas addition of BSA to this reaction had no effect on BAF-1 phosphorylation, addition of either human Lem4 aa 59–938 or *C. elegans* LEM-4L aa 257–600 strongly inhibited BAF-1 phosphorylation by VRK-1, as well as VRK-1 autophosphorylation (Figure 5B). To determine which domains of Lem4 are required for inhibition, we performed kinase assays in the presence of a number of Lem4 truncations (Figure 5C). Whereas Lem4 aa 59–938 strongly inhibited BAF-1 phosphorylation, removal of the LEM domain (to leave aa 114–938) resulted in a weaker effect, and Lem4 aa 442–938

Figure 2. *lem-4L(ax475)* Affects NE Structure and the Chromatin Recruitment of GFP-BAF-1 during Mitotic Exit

(A–F) TEMs of nuclei from embryos obtained from wild-type (n = 10) (A), *lem-4L(ax475)* grown at 16°C (n = 24) (B) and 25°C (n = 8) (C–D), *baf-1(t1639)* grown at 25°C (n = 30) (E), and *lem-4L(ax475); vrk-1(x1)* double mutant grown at 25°C (n = 14) (F). White arrows, chromatin not covered by NE. Scale bar, 2 μm.

(G–J) The first zygotic division of *control(RNAi)*, *lem-4L(RNAi)*, *lem-3(RNAi)*, *lem-2(RNAi)*, and *emr-1(RNAi) C. elegans* embryos expressing GFP-BAF-1 imaged using dual fluorescence and DIC microscopy. GFP-BAF-1 intensity represents the fluorescence intensity at the nuclear periphery divided by the cytoplasmic intensity after background subtraction. Error bars represent SD. At 80 s, in case of *lem-4L(RNAi)* $p = 7.78 \times 10^{-6}$, *lem-3(RNAi)* p = 0.046, *lem-2(RNAi)* p = 0.475, and *emr-1(RNAi)* p = 0.030 in t test relative to *control(RNAi)*.

(K and L) HeLa cells stably expressing H2B-mCherry and GFP-BAF were transfected with control, Lem4 oligo 1 or 2, Lem2, or Emerin siRNAs. After 48 hr, time-lapse microscopy was performed for 24 hr. GFP-BAF fluorescence intensity at the chromatin at each time point was measured and divided by the intensity at metaphase chromatin. Error bars represent SD. At 6 min, in case of (K) Lem4 RNAi #1 $p = 6.45 \times 10^{-26}$, Lem4 RNAi #2 $p = 2.54 \times 10^{-29}$, (L) Lem4 RNAi #1 $p = 4.02 \times 10^{-22}$, Lem2 RNAi p = 0.002, and Emerin p = 0.933 in t test relative to control RNAi.

See also Figure S3 and Table S3.

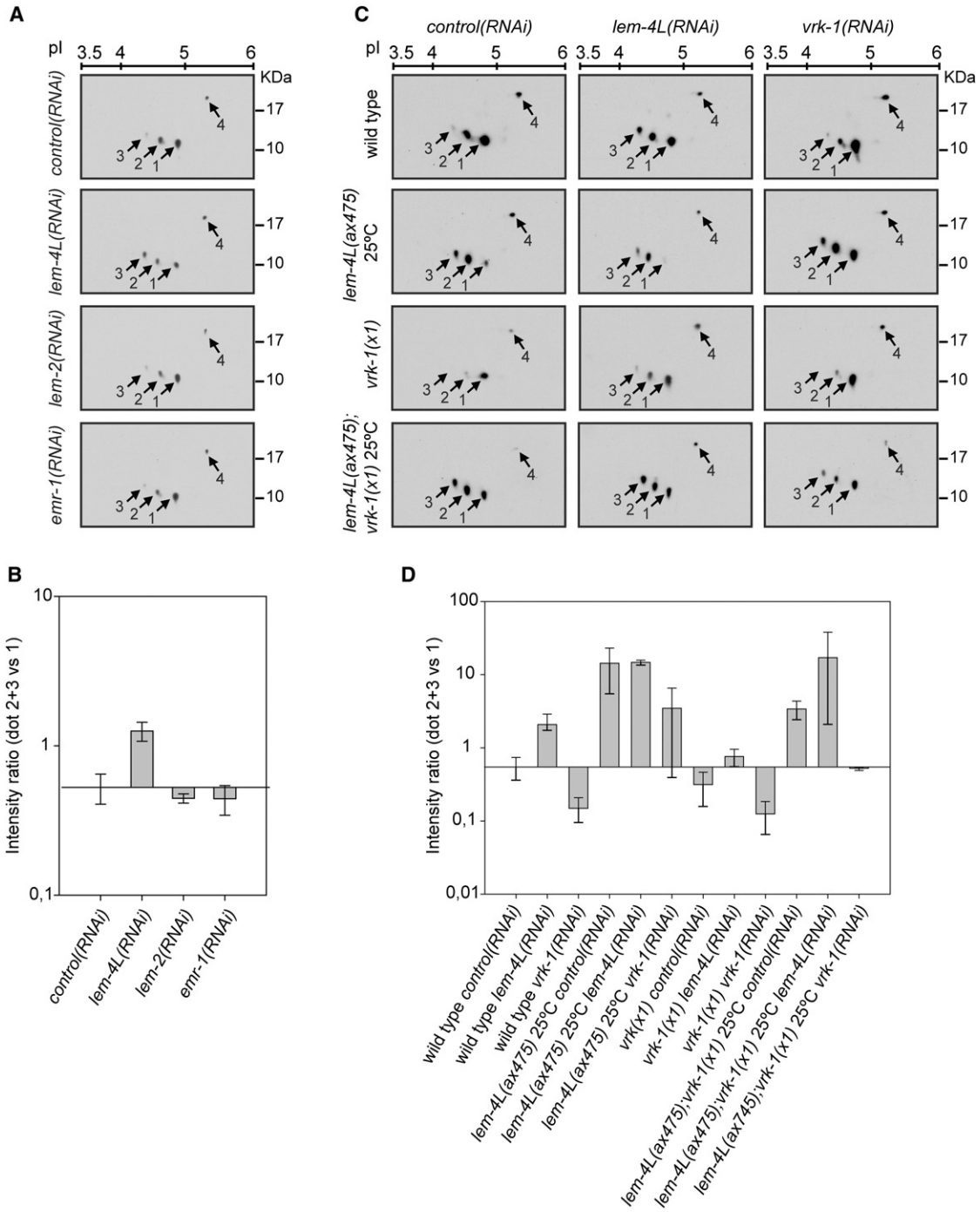

Figure 4. VRK-1 and LEM-4L Regulate BAF-1 Phosphorylation Divergently

(A) 10 μg protein extract from *control(RNAi)*, *lem-4L(RNAi)*, *lem-2(RNAi)*, and *emr-1(RNAi)* embryos was resolved in two dimensions and western blotted with anti-BAF-1. Isoelectric point (pI) is indicated above the panels, and molecular mass is indicated on the right. Arrows point to different BAF-1 isoforms.

(B) Measurement of the intensity ratio of phosphoisoforms 3+2 to isoform 1 from four independent experiments was used for quantitation. The intensity of spot 4 varied between experiments (Gorjánácz et al., 2007).

(C) Wild-type, *lem-4L(ax475)* mutant grown at 25°C, *vrk-1(x1)*, and *lem-4-like(ax475);vrk-1(x1)* double mutant at 25°C were subjected to control, *lem-4L*, or *vrk-1* RNAi for 48 hr. BAF-1 isoforms were visualized as in (A).

(D) Quantitation of BAF-1 phosphorylation as in (B). Error bars represent SD (B and D).

See also Table S2.

did not inhibit (Figure 5D). Due to poor solubility of various constructs, we were unable to test whether the ankyrin repeats of LEM-4L affect BAF-1 phosphorylation, but the N terminal aa 19–155 had no effect (Figure 5D). Lem4 aa 59–938 and LEM-4L aa 257–600 also blocked the phosphorylation of histone H3 by VRK-1 (Figure S4A), but not the phosphorylation of histone H1 by CDK1/cyclinB (Figure S4B).

Because Lem4 inhibited BAF-1 phosphorylation by VRK-1, we tested whether Lem4 could dephosphorylate BAF-1 in vitro. VRK-1 was immobilized on glutathione beads and incubated with BAF-1 in the presence of [γ^{32}P]-ATP. Immobilized VRK-1 was then removed, as visible from autophosphorylated VRK-1 (Figure 5E). Buffer alone, BSA, Lem4, or λ phosphatase was then added to the phosphorylated BAF-1. Lem4 aa 59–938 or LEM-4L aa 257–600 had no effect on BAF phosphorylation, whereas λ phosphatase efficiently removed radiolabeled phosphate (Figure 5E). These results suggest that Lem4 acts by interacting with VRK-1 and inhibiting VRK-1-mediated phosphorylation of BAF-1.

PP2A Dephosphorylates BAF-1 and Influences BAF Dynamics and NE Formation

Although Lem4 and LEM-4L are important for the recruitment of BAF to chromatin during mitotic exit and are able to inhibit BAF-1 phosphorylation by VRK-1, this does not explain BAF dephosphorylation upon exit from mitosis. Interestingly, Lem4 was identified as interacting with PP2A subunits. PP2A has been shown to be important for mitotic progression (Glatter et al., 2009; Bollen et al., 2009). PP2A mainly exists as a trimeric holoenzyme comprising a catalytic subunit (PP2A-CA or PP2A-CB), a scaffold subunit (PP2A-R1A or PP2A-R1B), and one of at least 15 specificity subunits (PP2A-B family members). To investigate Lem4 interaction with endogenous PP2A, lysates were prepared from asynchronously grown HeLa cells, and Lem4 or Lem2 as a control was immunoprecipitated (Figure 6A). A small fraction of PP2A-C and PP2A-R1 coimmunoprecipitated with Lem4, whereas Emerin and PP1-C did not, indicating that Lem4 interacts with endogenous PP2A, but not endogenous Emerin or PP1. Neither PP2A-C nor PP2A-R1 coimmunoprecipitated with Lem2, but PP1-C did (see Discussion).

We next tested direct PP2A-Lem4 interaction. We incubated GST-tagged Lem4 constructs or GST alone with either HeLa lysate or purified PP2A (Figure 6B). PP2A-C, PP2A-R1, and the regulatory subunit PP2A-B55α from HeLa lysate all bound to GST-Lem4 aa 59–938, but not to GST alone, GST-Lem4 aa 59–114 (LEM domain), or GST-Lem4 aa 349–442 (ankyrin repeats), whereas Emerin or mAb414-reactive nucleoporins did not bind to any. Purified PP2A also specifically bound to GST-Lem4 aa 59–938. Additional GST pull-down experiments mapped the PP2A binding region to amino acids 162–349 of Lem4 (Figure S5).

We wished to determine whether PP2A could directly dephosphorylate BAF-1 in vitro. Phosphorylated BAF-1 was prepared as described in Figure 5D and incubated in the presence of buffer alone, λ PPase, or purified human PP2A. Both PP2A and λ PPase dephosphorylated BAF-1 under these conditions (Figure 6C).

Because PP2A was found to interact with Lem4 and also to dephosphorylate BAF-1 in vitro, we next tested whether RNAi against a catalytic subunit of PP2A (PP2A-CA) affects the recruitment of BAF during anaphase. PP2A-CA depletion affected the recruitment of GFP-BAF to chromatin similarly to Lem4 depletion, whereas depletion of the catalytic subunit of protein phosphatase 1 (PP1-CA), which also regulates mitosis (Bollen et al., 2009), did not (Figure 6D, depletion efficiency S6K). A PP2A complex comprising PP2A-CA, PP2A-R1A, and PP2A-B55α has recently been shown to be essential for the progression from anaphase onset to NE formation (Schmitz et al., 2010), which is exactly when BAF dephosphorylation is expected to occur. We therefore depleted PP2A-CA, PP2A-R1A, and PP2A-B55α and monitored the recruitment of GFP-BAF to chromatin during mitotic exit. Depletion of PP2A-CA, PP2A-R1A, or PP2A-B55α all affected recruitment of GFP-BAF to chromatin (Figure 6E, depletion efficiency S6K), although depletion of PP2A-CA and PP2A-R1A affected GFP-BAF more than depletion of PP2A-B55α (Figure 6E). These results indicate that a PP2A complex comprising PP2A-CA, PP2A-R1A, and potentially PP2A-B55α regulates the recruitment of BAF to chromatin during mitotic exit in human cells.

To determine whether the effect of PP2A on BAF is evolutionarily conserved, we silenced *let-92* and *tag-93*, the *C. elegans* orthologs of human PP2A-C and PP2C-B, respectively, and monitored the anaphase chromatin recruitment of GFP-BAF-1. RNAi efficiency was controlled by western blotting (Figure S6J; data not shown). In *let-92(RNAi)* embryos, the anaphase recruitment of GFP-BAF-1 was strongly inhibited, whereas its intensity at the NE during interphase was unaffected (n = 10) (Figure 6F). In contrast, TAG-93 RNAi had no significant effect on the localization of GFP-BAF-1 (n = 8) (Figure 6F). We next depleted other PP2A subunits, including PAA-1 (n = 11), the sole PP2A structural subunit in *C. elegans*, and seven predicted PP2A regulatory subunits (*sur-6* [n = 23], *pptr-1* [n = 7], *pptr-2* [n = 13], *rsa-1* [n = 14], F47B8.3 [n = 10], T22D1.5 [n = 17], and C06G1.5 [n = 10]). As in human cells, depletion of the structural subunit PAA-1 resulted in a delay of GFP-BAF-1 recruitment similar to that observed upon depletion of the catalytic subunit LET-92 (Figures 6G, S6A, and S6B). Both *paa-1* and *let-92* were partially depleted to avoid potential pleiotropic effects associated with efficient downregulation of these genes in *C. elegans*. Furthermore, depletion of the PP2A-B55α ortholog SUR-6 resulted in a mild delay of GFP-BAF-1 recruitment, which is also similar to that seen in human cells (Figures 6G and S6C). Importantly, GFP-BAF-1 recruitment during mitotic exit was not delayed by depletion of any other regulatory subunits of PP2A (Figures S6D–S6I); however, it was slightly enhanced by depletion of *pptr-1*.

These findings prompted us to analyze BAF-1 phosphorylation. We compared the phosphorylation patterns in extracts prepared from control, *let-92*, *tag-93*, *paa-1*, *sur-6*, *rsa-1*, *pptr-1*, *pptr-2*, *CO6G1.5*, *F47B8.3*, *T22D1.5*, *lem-4L*, and *vrk-1* depleted embryos. We found that downregulation of *let-92* and *paa-1* resulted in increased phosphorylation of BAF-1 similar to that observed upon inactivation of *lem-4L* (Figures 6H, S6A, S6B, and S6J). Importantly, inactivation of *lem-4L* had no effect on their expression level (Figure S6J). Downregulation of *tag-93* and other PP2A subunits had no observable effect on BAF-1 phosphorylation (Figures 6H and S6J).

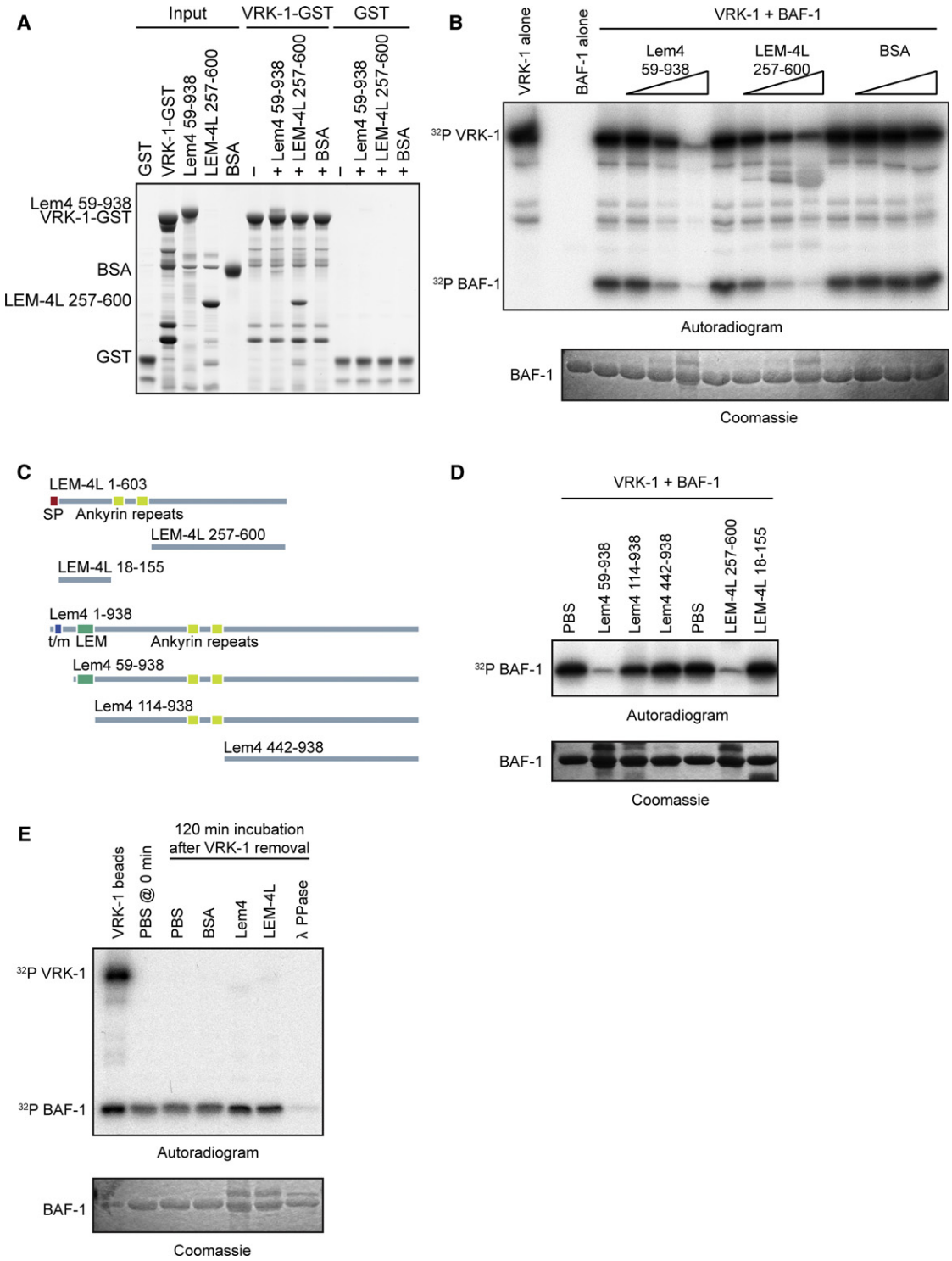

Figure 5. LEM-4L and Lem4 Inhibit VRK-1 Phosphorylation of BAF-1

(A) GST-VRK-1-His or GST alone was incubated with glutathione Sepharose 4B and His-Lem4 aa 59–938, His-LEM-4L aa 257–600, or bovine serum albumin (BSA). Bound proteins were eluted, separated by SDS-PAGE, and stained with Coomassie. Input and pull-down lanes, 10% of input or eluates.

(B) zz-BAF-1-His (15 μM) was incubated with GST-VRK-1-His (0.375 μM) in the presence of [γ-^{32}P]ATP and 0, 0.375, 3, or 15 μM of His-Lem4 aa 59–938, His-LEM-4L aa 257–600, or BSA for 2 hr and resolved by SDS-PAGE. Phosphorylated BAF and VRK1 were autoradiographed, and Coomassie-stained BAF is a loading control.

(C) Schematic representation of His-Lem4 truncations used in (D).

To confirm that the similar phenotype observed upon downregulation of *lem-4L* and *let-92* is due to a functional link in vivo, we performed a genetic interaction study in *C. elegans*. Because efficient downregulation of *let-92* resulted in 100% embryonic lethality, we performed partial RNAi-mediated downregulation of *let-92* in wild-type or mutant *lem-4L(ax475)* worms at 20°C. Progressive dilution of *let-92* RNAi treatment with control RNAi resulted in decreased embryonic lethality in wild-type embryos (Figure 7A). The same dilution steps, however, resulted in strongly enhanced embryonic lethality when combined with the partial inactivation of *lem-4L* in *lem-4L(ax475)* mutant worms at 20°C (Figure 7A). Combined silencing of *lem-4L* with the control phosphatase *tag-93* showed no synergistic effect (data not shown). This suggests that LEM-4L acts together with LET-92 (PP2A).

We next compared the NE phenotypes caused by inactivation or depletion of *lem-4L* and *let-92* by immunofluorescence and by TEM. We found that the nuclei in LET-92 depleted embryos closely resembled those in LEM-4L inactivated embryos. They were multilobed, and NPC-containing membranes were not organized into a closed NE rim, although they were partially associated with chromatin (Figures 7B–7D and S7A). The antagonistic functioning of PP2A and VRK-1 was further suggested by the finding that the embryonic lethality caused by *let-92* depletion was partially rescued by *vrk-1* codepletion, but not by codepletion of control genes (Figure S8).

These results demonstrate that inhibition of VRK-1 by Lem4/LEM-4L and dephosphorylation of BAF by PP2A are required for timely BAF recruitment to the nuclear periphery during anaphase, where it can exert its role in NE assembly.

DISCUSSION

The involvement of protein phosphorylation in the breakdown of the NE is well established, and several protein kinases and target proteins have been identified (Güttinger et al., 2009). This suggests that NE reassembly requires corresponding phosphatases that act on the same substrates, but examples were lacking. We characterize Lem4 and LEM-4L, related human and *C. elegans* proteins that are required for postmitotic NE assembly. Although LEM-4L has no recognizable LEM domain, the two proteins are related in sequence (BLAST e-value 10^{-41}) and appear to be functionally homologous. Both affect the modification state of the BAF protein, whose phosphorylation and dephosphorylation are required for NE breakdown and assembly, respectively. Recombinant forms of both proteins interact directly with and inhibit the BAF mitotic kinase, VRK-1. They both also interact physically and genetically with at least one PP2A complex and act together with PP2A to dephosphorylate BAF-1 (Figure 7E). In the absence of the Lem4 proteins, BAF-1 remains hyperphosphorylated and unable to carry out its essential function in NE reassembly. The Lem4 proteins are thus mitotic regulators that are important for the integrated regulation of a mitotic kinase and phosphatase to ensure coordinated exit from mitosis. They may provide an important prototype for how such coordination is achieved because it is generally the case that changes in both kinase and phosphatase activities are required to enable mitotic exit.

LEM-4 Inhibits VRK-1 Kinase Activity on BAF-1

The network of proteins at the nuclear periphery is essential for the interphase structure and function of the NE (Dauer and Worman, 2009). BAF, by binding to LEM proteins and chromatin, plays a central role in the maintenance of nuclear architecture in metazoa (Margalit et al., 2007). During mitotic entry, nucleoplasmic VRK-1 phosphorylates BAF and abrogates its molecular interactions, facilitating NE disassembly (Gorjánácz et al., 2007; Nichols et al., 2006). This suggests that, during mitotic exit, VRK-1 and BAF should be inactivated and dephosphorylated, respectively, in order to enable BAF to contribute to nuclear reformation. In mammals, but not in *C. elegans*, there is a reduction in VRK-1 protein level at mitotic exit (Kang et al., 2007; Gorjánácz et al., 2007), suggesting additional regulatory mechanisms. Our results demonstrate that Lem-4 and its *C. elegans* homolog LEM-4L are essential regulators of BAF phosphorylation by VRK-1 kinase and act by directly inhibiting the activity of the kinase. Further studies are needed to determine whether Lem4 also regulates other VRK paralogues (Klerkx et al., 2009). In both human cells and *C. elegans* embryos, Lem4 is detectable at the NE during its reformation (data not shown), which might suggest that it acts on VRK-1 at the reforming nuclear periphery. However, because the bulk of both VRK-1 and BAF-1 are soluble in the cytoplasm at this stage and because BAF is extremely mobile (Shimi et al., 2004), Lem4 inhibition may instead occur over the entire mitotic ER surface. Indeed, unlike LEM-4L and uniquely among LEM domain proteins, human Lem4 is not enriched at the NE during interphase but is uniformly distributed throughout the ER. The bulk of the protein is thus separated from both VRK-1 and BAF during interphase, and its inhibitory activity may only be required late in mitosis. Consistent with this idea, specific inactivation of *C. elegans* LEM-4L during mitosis, but not during interphase, gives rise to nuclear defects (Figures S7B–S7D).

Although both human and *C. elegans* genomes encode several LEM proteins (Wagner and Krohne, 2007), our results suggest that the role of Lem4 homologs in NE assembly is unique. Of the LEM domain proteins analyzed here, only Lem4/LEM-4L affected the mitotic localization and phosphorylation

(D) zz-BAF-1-His (10 μM) was incubated with GST-VRK-1-His (0.25 μM) in the presence of [γ-^{32}P]ATP and truncated forms of Lem4 (10 μM) for 2 hr and resolved by SDS-PAGE. Phosphorylated BAF-1 was autoradiographed, and Coomassie-stained BAF is a loading control.
(E) zz-BAF-1-His (20 μM) was incubated with GST-VRK-1-His-glutathione Sepharose 4B beads (1 μM VRK-1) in the presence of [γ-^{32}P]ATP. After 2 hr, GST-VRK-1-His-beads were removed and resuspended in SDS-PAGE sample buffer (lane 1). Phosphorylated BAF-1 (10 μM) was then incubated with His-Lem4 aa 59–938, His-LEM-4L aa 257–600, BSA (all 10 μM), λ phosphatase (400 units, 1 mM $MnCl_2$), or PBS. Reactions were stopped at 0 min or after 2 hr and resolved by SDS-PAGE. Phosphorylated BAF-1 and VRK-1 were autoradiographed, and Coomassie-stained BAF-1 is a loading control.
See also Figure S4 and Table S1.

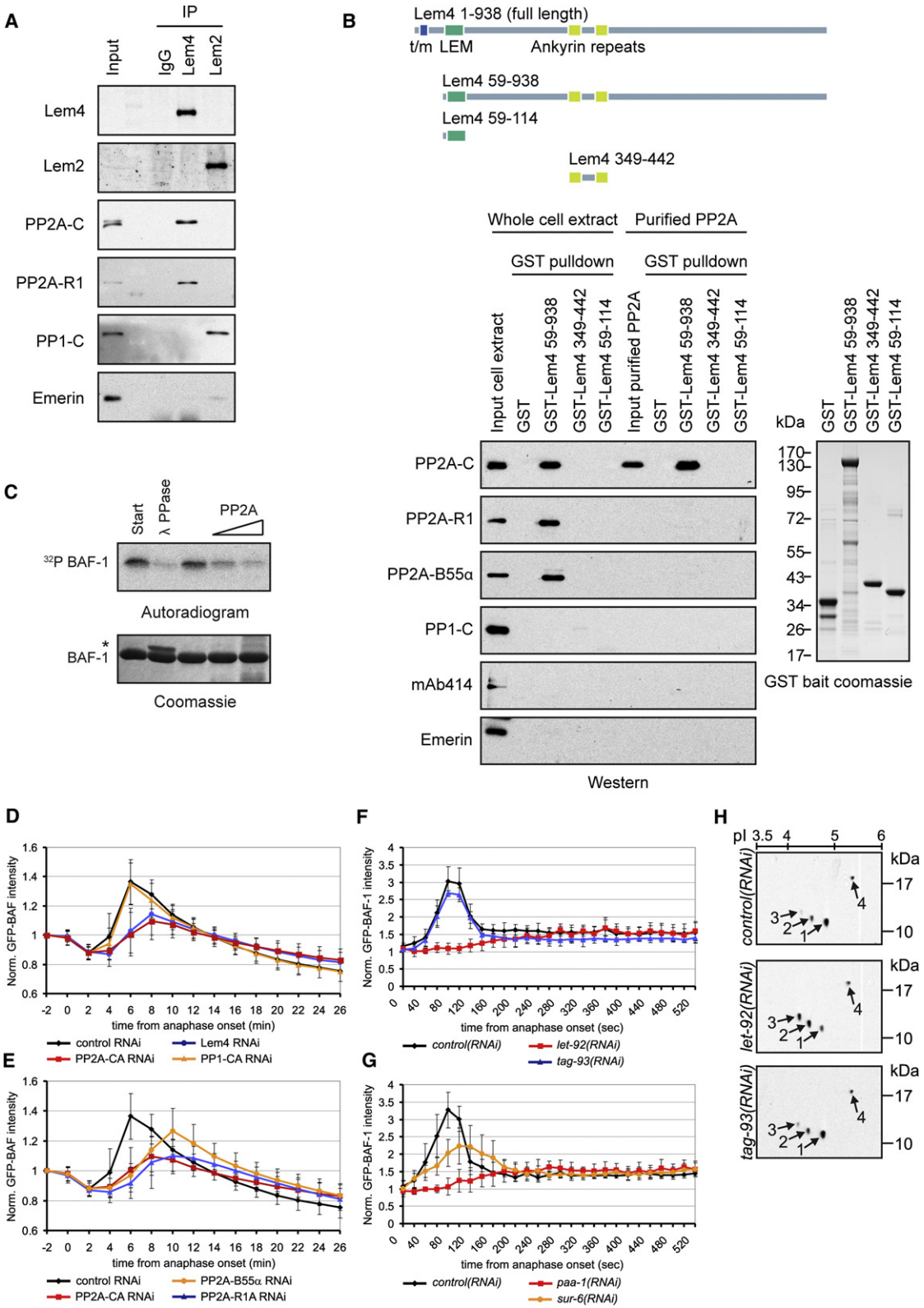

Figure 6. PP2A Dephosphorylates BAF-1 and Influences Its Recruitment to Chromatin upon Mitotic Exit

(A) Lem4 and Lem2 were immunoprecipitated from HeLa cell lysate. Immunoprecipitates were separated by SDS-PAGE and processed for western blotting with Lem4, Lem2, PP2A-C, PP2A-R1, PP1-C, and Emerin antibodies. Input, 0.03% of immunoprecipitation (IP) input. IP lanes, 20% of eluates.

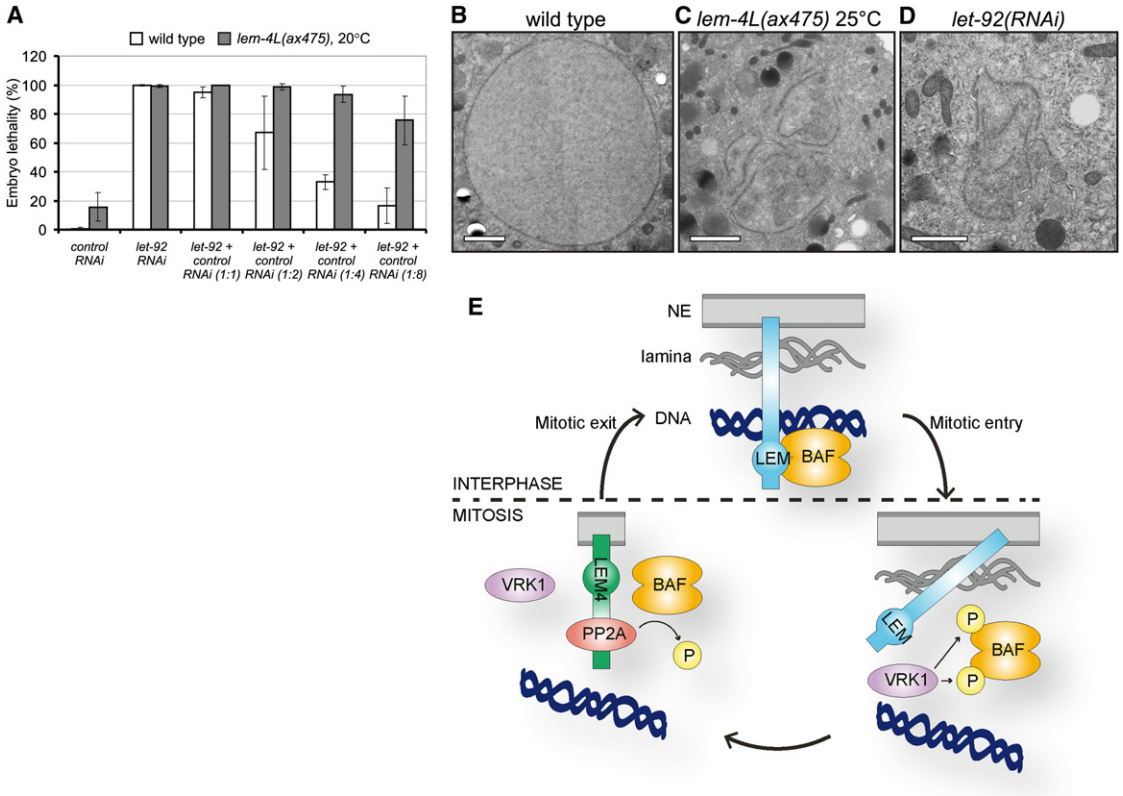

Figure 7. *lem-4L* and *let-92* Genetically Interact, and Their Depletion Results in Similar NE Defects

(A–D) Genetic interaction between *lem-4L* and *let-92* was detected by a synthetic lethality effect upon partial reduction of LEM-4L and LET-92 during 24- to 33-hr-long RNAi treatments. Wild-type and temperature-sensitive *lem-4L(ax475)* mutant worms were subjected to *control(RNAi)*, *let-92(RNAi)* diluted 1:1, 1:2, 1:4, and 1:8 with control RNAi at 20°C. Embryonic lethality was determined in three independent experiments. Error bars represent SD. NE structure was analyzed by TEM in wild-type (n = 11) (B), *lem-4L(ax475)* (n = 8) (C), and *let-92(RNAi)* embryos (n = 20) (D), all at 25°C. Scale bars, 1 μm.

(E) Model of the evolutionarily conserved mechanism that regulates the function of BAF during nuclear assembly and disassembly.

See also Figures S7 and S8.

state of BAF and, while the *lem-4L* gene is essential in *C. elegans*, homozygous null *lem-2* or *emr-1* worms are fully viable. Lem4 is also the only LEM protein that copurifies with PP2A (Glatter et al., 2009).

Nevertheless, depletion of human Lem2 results in NE defects similar to those seen after Lem4 depletion (Ulbert et al., 2006). Although Lem2 does not interact with PP2A, we observed that PP1-CA coimmunoprecipitated with Lem2. PP1 is involved in

(B) GST alone or GST-Lem4 fragments were incubated with glutathione Sepharose 4B and either HeLa cell extract or purified PP2A. Bound proteins were eluted, separated by SDS-PAGE, and processed for western blotting with PP2A-C, PP2A-R1, PP2A-B55α, PP1-C, and Emerin antibodies. Input, 0.6% of IP input. Pull-down lanes, 10% of eluates. GST baits were separated by SDS-PAGE and stained with Coomassie.

(C) zz-BAF-1-His (40 μM) was incubated with GST-VRK-1-His-glutathione Sepharose 4B beads (1 μM VRK-1) in the presence of [γ-^{32}P]ATP. After 2 hr, GST-VRK1-His-beads were removed. Phosphorylated BAF-1 (10 μM) was then incubated with PBS, λ phosphatase (400 units), or purified PP2A (0.02, 0.075 units) in phosphatase buffer. Remaining reactions were stopped at 0 min or after 2 hr and resolved by SDS-PAGE. Phosphorylated BAF-1 was autoradiographed, and Coomassie-stained BAF-1 is a loading control. Asterisk, λPPase.

(D and E) HeLa cells stably expressing H2B-mCherry and GFP-BAF were transfected with control, Lem4 oligo 1, PP2A-CA, PP1-CA, PP2A-R1A, or PP2A-B55α siRNAs. After 48 hr, time-lapse microscopy was performed for 24 hr. GFP-BAF intensity was quantified. Error bars represent SD. At 6 min, in case of Lem4 RNAi #1 $p = 4.02 \times 10^{-22}$, PP2A-CA RNAi $p = 2.42 \times 10^{-38}$, PP1-CA RNAi $p = 0.633$, PP2A-R1A RNAi $p = 4.54 \times 10^{-33}$, and PP2A-B55α $p = 5.03 \times 10^{-31}$ in t test relative to control RNAi.

(F and G) The first zygotic division of *control(RNAi)*, *let-92(RNAi)*, tag-93*(RNAi)*, *paa-1(RNAi)*, and *sur-6(RNAi) C. elegans* embryos expressing GFP-BAF-1 imaged using dual fluorescence and DIC microscopy. GFP-BAF-1 intensity at the nuclear periphery was quantified. Error bars represent SD. At 80 s time point, in case of *let-92(RNAi)* $p = 1.66 \times 10^{-6}$, *tag-93(RNAi)* $p = 0.011$, *paa-1(RNAi)* $p = 4.61 \times 10^{-10}$, and *sur-6(RNAi)* $p = 1.57 \times 10^{-6}$ in t test relative to the *control(RNAi)*.

(H) 10 μg protein extract from *control(RNAi)*, *let-92(RNAi)*, and *tag-93(RNAi)* embryos was resolved in two dimensions; western blotting with anti-BAF-1. pI is indicated above the panels, and molecular mass is indicated on the left. Arrows point to BAF-1 isoforms. Phosphorylation of BAF-1 was quantified as the ratio of the intensity of spot 2+3 versus dot 1 from three different experiments. The observed ratios were: *control(RNAi)* 0.41 ± 0.12; *let-92(RNAi)* 1.92 ± 1.44; and *tag-93(RNAi)* 0.45 ± 0.05.

See also Figures S5 and S6 and Tables S1, S2, and S3.

the regulation of a number of mitotic processes (Bollen et al., 2009; Wurzenberger and Gerlich, 2011). The effect of Lem2 on PP1 is therefore worth investigating.

PP2A Promotes NE Assembly by Dephosphorylating BAF-1

Regulated phosphorylation is crucial for mitotic NE dynamics and requires not only degradation or inhibition of mitotic kinases at the stage at which they are no longer required but also the activity of protein phosphatases. A PP2A complex comprising PP2A-CA, PP2A-R1A, and PP2A-B55α is essential in human cells for the progression from anaphase to NE formation (Schmitz et al., 2010). Although this complex acts downstream of cyclin-dependent kinase (CDK) inactivation, its targets were unknown (Schmitz et al., 2010). The same PP2A trimeric holoenzyme has recently been shown to control centriole formation in *C. elegans* (Kitagawa et al., 2011; Song et al., 2011).

In this paper, we provide evidence that PP2A plays a role in NE assembly and identify BAF as a PP2A target. Both *C. elegans* and human PP2A complexes comprising PP2A-CA, PP2A-R1A, and potentially PP2A-B55α are required to dephosphorylate BAF during mitotic exit and thus allow its efficient recruitment to chromatin and interaction with other components of the nuclear periphery. Whereas downregulation of human PP2A-CA, PP2A-R1A, or the *C. elegans* PP2A-C and PP2A-R1 homologs delayed and reduced the level of BAF recruitment to chromatin, depletion of PP2A-B55α or its *C. elegans* homolog delayed but did not strongly reduce its binding. It is possible that incomplete depletion of PP2A-B55α is responsible for this difference. However, it might also be that another regulatory subunit is partially redundant with PP2A-B55α in BAF dephosphorylation or that the mild effect of PP2A-B55α depletion on GFP-BAF chromatin recruitment may instead be an indirect consequence of its role in mitotic exit (Schmitz et al., 2010).

There is also a possibility that Lem4/LEM-4L may itself act as a regulatory subunit with PP2A-C/R1 dimers. In support of this idea, Lem4 directly interacted with purified PP2A and, like a number of phosphatase regulatory subunits, contained ankyrin repeats (Browne et al., 2007; Stefansson et al., 2008 and references therein). Further, BAF-1 phosphorylation was unaffected by depletion of any of known *C. elegans* PP2A regulatory subunits, whereas depletion of Lem4/LEM-4L phenocopied the depletion of catalytic or structural subunits of PP2A.

Apart from the inhibitory effect of Lem4 on VRK-1, the similar effect on BAF recruitment caused by Lem4 and PP2A depletion and their genetic interaction strongly suggests that Lem4 also plays an active role with PP2A to bring about BAF-1 dephosphorylation. This double role in NE assembly is analogous to the proposed functions of A-kinase anchor proteins (AKAP) in protein-kinase-A-mediated signaling events. Some AKAP proteins bind both PKAs and protein phosphatases and are thought to regulate phosphorylation cycle dynamics (Colledge and Scott, 1999).

Our study of the Lem4 proteins has led to a more integrated picture of the control of BAF phosphorylation during mitosis. Further study is needed to understand what causes the interaction of Lem4 proteins with VRK-1 kinase and PP2A phosphatase activities to change during the course of mitosis to bring about timely NE assembly.

EXPERIMENTAL PROCEDURES

See also Supplemental Information.

Live-Cell Imaging

C. elegans embryos were mounted between a coverslip and a 2% agar pad and analyzed by dual differential interference contrast (DIC) and fluorescence confocal microscopy with Leica SP2 and SP5 microscopes using a 63× Plan-Apochromat oil objective. Images were acquired every 20 s. Temperature shift experiments utilized a ministage temperature controller (Gorjánácz et al., 2007).

HeLa cells stably expressing H2B-mCherry and GFP-BAF were seeded on Labtek chambered coverslips (Nunc, 7,500 cells per well) and incubated with RNAi transfection mixture (see Extended Experimental Procedures). After 48 hr, imaging medium (78% [v/v] CO_2-independent medium [GIBCO], 20% [v/v] fetal bovine serum, 2 mM L-glutamine, 100 μg/ml penicillin/streptomycin) was added and sealed with silicon grease. Epifluorescence images were acquired every 2 min by using an Olympus Europe IX-81 automated microscope and a 10× Plan-Apochromat objective (NA 0.4) in a custom microscope incubator. A custom version of ScanR, including an autofocus routine, was used (Neumann et al., 2006).

VRK-1 Kinase Assay

zz-BAF-1-His was mixed with GST-VRK-1-His at a 40:1 molar ratio in 20 mM Tris [pH 7.5], 5 mM $MgCl_2$, 50 mM NaCl, and 1 mM DTT, plus protease inhibitors (Roche Complete, EDTA). Reaction volume was 12.5 μl. Reactions were initiated with 0.125 μl of 10 μCi/μl [γ-32P]ATP (Hartmann Analytic) and incubated at room temperature for 2 hr, and SDS-PAGE sample buffer was added. Proteins were resolved by 14% SDS-PAGE, and phosphorylation was detected by autoradiography.

For phosphatase assays, ~10 μg GST-VRK-1-His was incubated with 25 μl glutathione Sepharose 4B beads (GE Healthcare) in PBS for 1 hr at room temperature. Beads were washed with PBS and equilibrated in kinase buffer. GST-VRK-1-His-glutathione Sepharose 4B beads were then mixed with zz-BAF-1-His in a 1:40 molar ratio. Phosphorylated zz-BAF-1-His was separated from GST-VRK-1-His beads by using a Mobicol column (MoBiTec); 2.5 μl of phosphorylated zz-BAF-1-His was used as a phosphatase substrate in a 20 μl reaction in either kinase buffer or phosphatase buffer: 50 mM imidazole [pH 7.2], 1 mM EDTA, 1 mM EGTA, 0.02% β-mercaptoethanol, 0.1 mg/ml BSA, and protease inhibitors (Roche Complete, EDTA). Reactions were incubated at room temperature for 2 hr, and SDS-PAGE sample buffer was added. Proteins were resolved by 14% SDS-PAGE, and phosphorylation was detected by autoradiography.

SUPPLEMENTAL INFORMATION

Supplemental Information includes Extended Experimental Procedures, eight figures, and three tables and can be found with this article online at http://dx.doi.org/10.1016/j.cell.2012.04.043.

ACKNOWLEDGMENTS

We thank Tokuko Haraguchi for GFP-BAF plasmid; Toby Gibson, Norman Davey, and Damien Devos for bioinformatics assistance; Ulrike Bauer and Victoria McParland for technical assistance; Stefan Leicht for help with 2D gels; and members of the Advanced Light Microscopy Facility (EMBL Heidelberg) for microscopy help. We thank Jan Ellenberg, Péter Lénárt, Maja Köhn, Geraldine Seydoux, Boris Bryk, and the Mattaj lab for comments on the manuscript. The NIH-funded Caenorhabditis Genetic Center provided some *C. elegans* strains. I.F.D. was an EMBO Long-Term Fellow, C.A. a Spanish Ministry of Science and Innovation Fellow, and M.G. a Human Frontier Science Program Organization Fellow.

Received: October 5, 2011
Revised: February 9, 2012
Accepted: April 20, 2012
Published: July 5, 2012

REFERENCES

Askjaer, P., Galy, V., Hannak, E., and Mattaj, I.W. (2002). Ran GTPase cycle and importins alpha and beta are essential for spindle formation and nuclear envelope assembly in living Caenorhabditis elegans embryos. Mol. Biol. Cell *13*, 4355–4370.

Bollen, M., Gerlich, D.W., and Lesage, B. (2009). Mitotic phosphatases: from entry guards to exit guides. Trends Cell Biol. *19*, 531–541.

Breitkreutz, A., Choi, H., Sharom, J.R., Boucher, L., Neduva, V., Larsen, B., Lin, Z.-Y., Breitkreutz, B.-J., Stark, C., Liu, G., et al. (2010). A global protein kinase and phosphatase interaction network in yeast. Science *328*, 1043–1046.

Browne, G.J., Fardilha, M., Oxenham, S.K., Wu, W., Helps, N.R., da Cruz E Silva, O.A., Cohen, P.T., and da Cruz E Silva, E.F. (2007). SARP, a new alternatively spliced protein phosphatase 1 and DNA interacting protein. Biochem. J. *402*, 187–196.

Burke, B., and Ellenberg, J. (2002). Remodelling the walls of the nucleus. Nat. Rev. Mol. Cell Biol. *3*, 487–497.

Colledge, M., and Scott, J.D. (1999). AKAPs: from structure to function. Trends Cell Biol. *9*, 216–221.

Dauer, W.T., and Worman, H.J. (2009). The nuclear envelope as a signaling node in development and disease. Dev. Cell *17*, 626–638.

Fernandez, A.G., and Piano, F. (2006). MEL-28 is downstream of the Ran cycle and is required for nuclear-envelope function and chromatin maintenance. Curr. Biol. *16*, 1757–1763.

Franz, C., Askjaer, P., Antonin, W., Iglesias, C.L., Haselmann, U., Schelder, M., de Marco, A., Wilm, M., Antony, C., and Mattaj, I.W. (2005). Nup155 regulates nuclear envelope and nuclear pore complex formation in nematodes and vertebrates. EMBO J. *24*, 3519–3531.

Galy, V., Mattaj, I.W., and Askjaer, P. (2003). Caenorhabditis elegans nucleoporins Nup93 and Nup205 determine the limit of nuclear pore complex size exclusion in vivo. Mol. Biol. Cell *14*, 5104–5115.

Galy, V., Askjaer, P., Franz, C., López-Iglesias, C., and Mattaj, I.W. (2006). MEL-28, a novel nuclear-envelope and kinetochore protein essential for zygotic nuclear-envelope assembly in C. elegans. Curr. Biol. *16*, 1748–1756.

Glatter, T., Wepf, A., Aebersold, R., and Gstaiger, M. (2009). An integrated workflow for charting the human interaction proteome: insights into the PP2A system. Mol. Syst. Biol. *5*, 237.

Golden, A., Sadler, P.L., Wallenfang, M.R., Schumacher, J.M., Hamill, D.R., Bates, G., Bowerman, B., Seydoux, G., and Shakes, D.C. (2000). Metaphase to anaphase (mat) transition-defective mutants in Caenorhabditis elegans. J. Cell Biol. *151*, 1469–1482.

Gorjánácz, M., Klerkx, E.P.F., Galy, V., Santarella, R., López-Iglesias, C., Askjaer, P., and Mattaj, I.W. (2007). Caenorhabditis elegans BAF-1 and its kinase VRK-1 participate directly in post-mitotic nuclear envelope assembly. EMBO J. *26*, 132–143.

Güttinger, S., Laurell, E., and Kutay, U. (2009). Orchestrating nuclear envelope disassembly and reassembly during mitosis. Nat. Rev. Mol. Cell Biol. *10*, 178–191.

Haraguchi, T., Koujin, T., Segura-Totten, M., Lee, K.K., Matsuoka, Y., Yoneda, Y., Wilson, K.L., and Hiraoka, Y. (2001). BAF is required for emerin assembly into the reforming nuclear envelope. J. Cell Sci. *114*, 4575–4585.

Haraguchi, T., Kojidani, T., Koujin, T., Shimi, T., Osakada, H., Mori, C., Yamamoto, A., and Hiraoka, Y. (2008). Live cell imaging and electron microscopy reveal dynamic processes of BAF-directed nuclear envelope assembly. J. Cell Sci. *121*, 2540–2554.

Hetzer, M.W., Walther, T.C., and Mattaj, I.W. (2005). Pushing the envelope: structure, function, and dynamics of the nuclear periphery. Annu. Rev. Cell Dev. Biol. *21*, 347–380.

Kang, T.-H., Park, D.-Y., Choi, Y.H., Kim, K.-J., Yoon, H.S., and Kim, K.-T. (2007). Mitotic histone H3 phosphorylation by vaccinia-related kinase 1 in mammalian cells. Mol. Cell. Biol. *27*, 8533–8546.

Kitagawa, D., Flückiger, I., Polanowska, J., Keller, D., Reboul, J., and Gönczy, P. (2011). PP2A phosphatase acts upon SAS-5 to ensure centriole formation in C. elegans embryos. Dev. Cell *20*, 550–562.

Klerkx, E.P.F., Alarcón, P., Waters, K., Reinke, V., Sternberg, P.W., and Askjaer, P. (2009). Protein kinase VRK-1 regulates cell invasion and EGL-17/FGF signaling in Caenorhabditis elegans. Dev. Biol. *335*, 12–21.

Lancaster, O.M., Cullen, C.F., and Ohkura, H. (2007). NHK-1 phosphorylates BAF to allow karyosome formation in the Drosophila oocyte nucleus. J. Cell Biol. *179*, 817–824.

Lin, F., Blake, D.L., Callebaut, I., Skerjanc, I.S., Holmer, L., McBurney, M.W., Paulin-Levasseur, M., and Worman, H.J. (2000). MAN1, an inner nuclear membrane protein that shares the LEM domain with lamina-associated polypeptide 2 and emerin. J. Biol. Chem. *275*, 4840–4847.

Margalit, A., Segura-Totten, M., Gruenbaum, Y., and Wilson, K.L. (2005). Barrier-to-autointegration factor is required to segregate and enclose chromosomes within the nuclear envelope and assemble the nuclear lamina. Proc. Natl. Acad. Sci. USA *102*, 3290–3295.

Margalit, A., Brachner, A., Gotzmann, J., Foisner, R., and Gruenbaum, Y. (2007). Barrier-to-autointegration factor—a BAFfling little protein. Trends Cell Biol. *17*, 202–208.

Neumann, B., Held, M., Liebel, U., Erfle, H., Rogers, P., Pepperkok, R., and Ellenberg, J. (2006). High-throughput RNAi screening by time-lapse imaging of live human cells. Nat. Methods *3*, 385–390.

Nichols, R.J., Wiebe, M.S., and Traktman, P. (2006). The vaccinia-related kinases phosphorylate the N′ terminus of BAF, regulating its interaction with DNA and its retention in the nucleus. Mol. Biol. Cell *17*, 2451–2464.

Schmitz, M.H.A., Held, M., Janssens, V., Hutchins, J.R.A., Hudecz, O., Ivanova, E., Goris, J., Trinkle-Mulcahy, L., Lamond, A.I., Poser, I., et al. (2010). Live-cell imaging RNAi screen identifies PP2A-B55alpha and importin-beta1 as key mitotic exit regulators in human cells. Nat. Cell Biol. *12*, 886–893.

Shimi, T., Koujin, T., Segura-Totten, M., Wilson, K.L., Haraguchi, T., and Hiraoka, Y. (2004). Dynamic interaction between BAF and emerin revealed by FRAP, FLIP, and FRET analyses in living HeLa cells. J. Struct. Biol. *147*, 31–41.

Song, M.H., Liu, Y., Anderson, D.E., Jahng, W.J., and O'Connell, K.F. (2011). Protein phosphatase 2A-SUR-6/B55 regulates centriole duplication in C. elegans by controlling the levels of centriole assembly factors. Dev. Cell *20*, 563–571.

Stefansson, B., Ohama, T., Daugherty, A.E., and Brautigan, D.L. (2008). Protein phosphatase 6 regulatory subunits composed of ankyrin repeat domains. Biochemistry *47*, 1442–1451.

Ulbert, S., Antonin, W., Platani, M., and Mattaj, I.W. (2006). The inner nuclear membrane protein Lem2 is critical for normal nuclear envelope morphology. FEBS Lett. *580*, 6435–6441.

Vagnarelli, P., Ribeiro, S., Sennels, L., Sanchez-Pulido, L., de Lima Alves, F., Verheyen, T., Kelly, D.A., Ponting, C.P., Rappsilber, J., and Earnshaw, W.C. (2011). Repo-Man coordinates chromosomal reorganization with nuclear envelope reassembly during mitotic exit. Dev. Cell *21*, 328–342.

Wagner, N., and Krohne, G. (2007). LEM-Domain proteins: new insights into lamin-interacting proteins. Int. Rev. Cytol. *261*, 1–46.

Wurzenberger, C., and Gerlich, D.W. (2011). Phosphatases: providing safe passage through mitotic exit. Nat. Rev. Mol. Cell Biol. *12*, 469–482.